Volume 12
Number 31
21 August 2021
Pages 10399–10674

Chemical Science

rsc.li/chemical-science

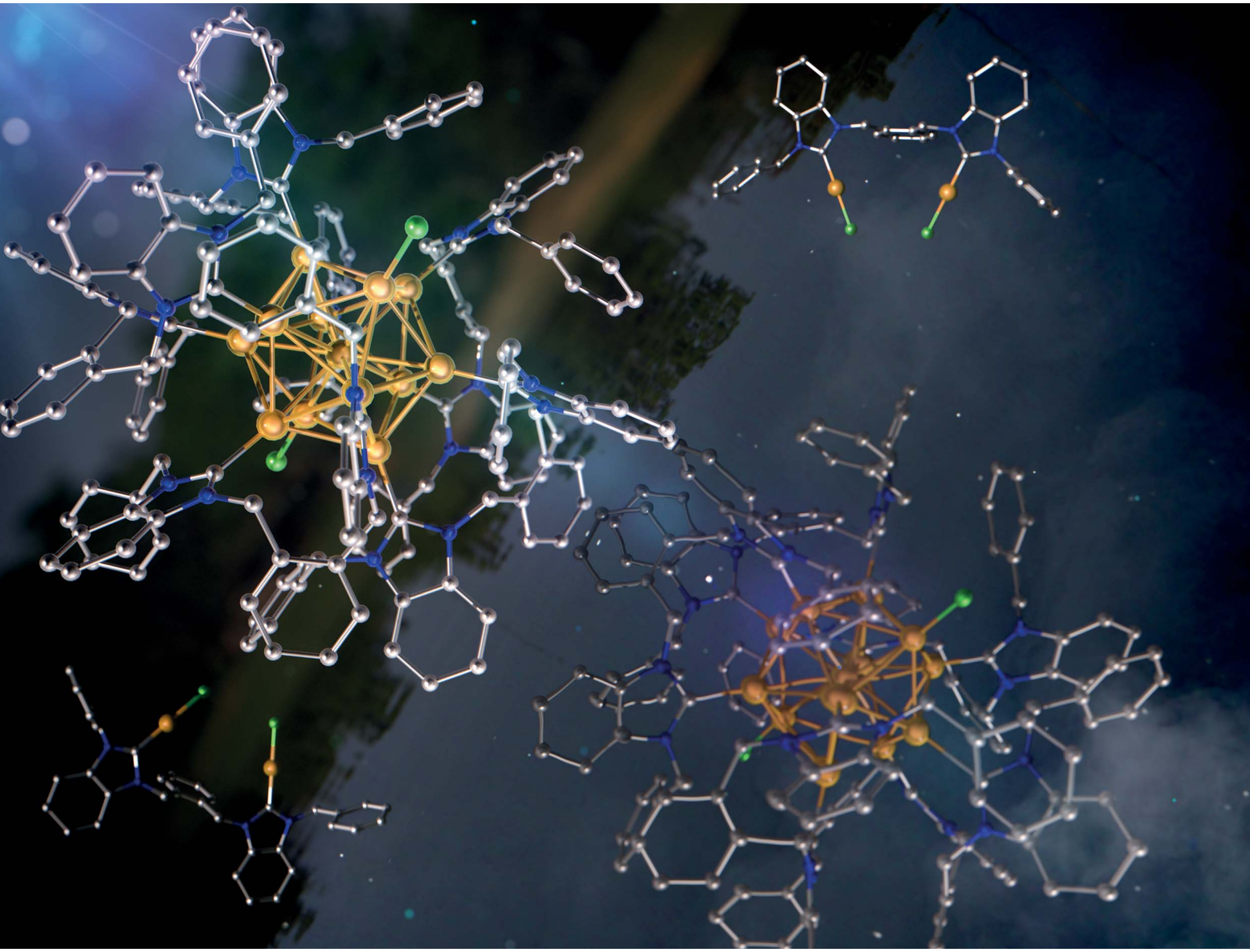

ISSN 2041-6539

ROYAL SOCIETY
OF **CHEMISTRY**

EDGE ARTICLE

Yoshitaka Aramaki, Takashi Ooi, Masakazu Nambo,
Cathleen M. Crudden *et al.*

Synthesis and enantioseparation of chiral Au_{13} nanoclusters
protected by bis-*N*-heterocyclic carbene ligands

Chemical Science

ROYAL SOCIETY OF CHEMISTRY

EDGE ARTICLE

View Article Online
View Journal | View Issue

Check for updates

Cite this: Chem. Sci., 2021, **12**, 10436

All publication charges for this article have been paid for by the Royal Society of Chemistry

Synthesis and enantioseparation of chiral Au_{13} nanoclusters protected by bis-*N*-heterocyclic carbene ligands†

Hong Yi, ‡[a] Kimberly M. Osten, ‡[a] Tetyana I. Levchenko,[b] Alex J. Veinot,[b] Yoshitaka Aramaki, *[ac] Takashi Ooi, *[ac] Masakazu Nambo *[a] and Cathleen M. Crudden *[ab]

Received 2nd June 2021
Accepted 27th June 2021

DOI: 10.1039/d1sc03076k

rsc.li/chemical-science

A series of chiral Au_{13} nanoclusters were synthesized *via* the direct reduction of achiral dinuclear Au(I) halide complexes ligated by *ortho*-xylyl-linked bis-*N*-heterocyclic carbene (NHC) ligands. A broad range of functional groups are tolerated as wingtip substituents, allowing for the synthesis of a variety of functionalized chiral Au_{13} nanoclusters. Single crystal X-ray crystallography confirmed the molecular formula to be $[Au_{13}(bisNHC)_5Cl_2]Cl_3$, with a chiral helical arrangement of the five bidentate NHC ligands around the icosahedral Au_{13} core. This Au_{13} nanocluster is highly luminescent, with a quantum yield of 23%. The two enantiomers of the Au_{13} clusters can be separated by chiral HPLC, and the isolated enantiomers were characterized by circular dichroism spectroscopy. The clusters show remarkable stability, including configurational stability, opening the door to further investigation of the effect of chirality on these clusters.

The intersection of chirality with nanomaterials has been called "one of the most dynamic areas in modern science".[1a] Atomically precise nanoclusters are a particularly important class of nanomaterials in this area because of the ability to discern molecular structure with high precision, and the high structural purity obtainable.[1] The unique properties of these nanomaterials opens up applications in chiral sensing,[2] enantioselective nanocatalysis[3] and chiroptics.[4] Chirality in metal nanoclusters can be generated *via* an intrinsically chiral metal core,[5] from an achiral core with chiral organic ligands[6] or from an achiral core with achiral ligands that are arranged in an asymmetric fashion.[7] Although impressive strides have been made in the synthesis of chiral metal clusters, considerable challenges remain with regards to designing chiral nanoclusters with stable chirality that is resistant to racemization and with optimized properties, for example photo-physical properties.

The Bürgi group have been pioneers in the creation of chiral thiolate-stabilized nanoclusters, highlighted by their work with $Au_{38}(SR)_{24}$, which is chiral by virtue of the arrangement of thiol staples around the core, and can be separated into its enantiomers by HPLC.[8] Cluster $Au_{38}(SCH_2CH_2Ph)_{24}$ shows high stability at room temperature, with racemization occurring in approximately 30 minutes at 80 °C.[9] Computational work from the Häkkinen group suggests that chiral inversions for $Au_{38}(SR)_{24}$ and Pd-doped Au_{38} can take place through a rotational reconstruction of the metal core without the need for ligand–metal bond cleavage.[10]

Smaller Au_{13} nanoclusters can also be prepared with achiral phosphine ligands depending on their orientation around the core. Shichibu and Konishi described this situation for $[Au_{13}(dppe)_5Cl_5]^{3+}$ (dppe = 1,2-bis(diphenylphosphino)ethane),[11] in which the five dppe ligands take up a propeller-like arrangement.[12] However, successful resolution of the individual enantiomers by chiral HPLC was not achieved, possibly due to fast racemization of these clusters in solution. The only examples of resolvable chiral Au clusters stabilized by phosphine ligands require the use of inherently chiral ligands.[13]

N-Heterocyclic carbenes (NHCs) have recently emerged as valuable alternatives to thiols or phosphines for the stabilization of metal surfaces, nanoparticles, and clusters.[14] The neutral, electron-rich NHCs form a strong covalent bond with the metal,[15] which is important in providing stability to metal nanoclusters.[16] Our group recently described the utility of NHCs in protecting gold nanoclusters, reporting the first examples of

---

[a] *Institute of Transformative Bio-Molecules (WPI-ITbM), Nagoya University Furo, Chikusa, Nagoya 464-8602, Japan. E-mail: aramaki@chembio.nagoya-u.ac.jp; tooi@chembio.nagoya-u.ac.jp; mnambo@itbm.nagoya-u.ac.jp; cruddenc@chem.queensu.ca*

[b] *Department of Chemistry, Queen's University, Chernoff Hall, Kingston, Ontario K7L 3N6, Canada*

[c] *Department of Molecular and Macromolecular Chemistry, Graduate School of Engineering, Nagoya University, Nagoya 464-8601, Japan*

† Electronic supplementary information (ESI) available. CCDC 2067324. For ESI and crystallographic data in CIF or other electronic format see DOI: 10.1039/d1sc03076k

‡ Hong Yi and Kimberly M. Osten contributed equally to this work.

NHC-containing Au_{11} and Au_{13} clusters.[17,18] Zheng *et al.* have also described the synthesis of Au_{13},[19] Au_{25} (ref. 20*a*) and Au_{44} (ref. 20*b*) nanoclusters, and Tsukuda has prepared Au_{23} clusters,[21] illustrating the potential of NHCs as stabilizing ligands for a range of gold nanocluster architectures. Very recently, Zang *et al.* reported the synthesis of Au_{11} and Au_{13} nanoclusters protected by *m*-phenylene-bridged *N*-heterocyclic carbene ligands that result in different clusters based on subtle changes in *N*-substituents.[22]

Herein we report the synthesis of chiral Au_{13} nanoclusters prepared with achiral bidentate NHC ligands. The nanoclusters derive their chirality from a helical arrangement of the achiral ligand (Fig. 1). The stability introduced by the NHC ligand permits the separation of the nanocluster into its constituent enantiomers by chiral HPLC. Each enantiomer was characterized by circular dichroism. The clusters display impressive thermal stability and record-setting photoluminescent quantum yields.

Inspired by the work of Zheng, who showed that bisNHC ligands linked by a simple propyl chain can provide stable Au_{13} nanoclusters,[19] we set out to examine bis-benzimidazolylidene ligands with aromatic linkers, designed to take advantage of the multitude of CH-π interactions observed in other Au_{13} clusters.[18] Bis-benzimidazolium salts (**1a–g**) prepared by simple $\mathrm{S_N2}$ reactions were converted into the corresponding Au complexes $(\mathrm{bisNHC})\mathrm{Au}_2\mathrm{X}_2$ (**2a–g**) by reaction with $\mathrm{Au(SMe_2)Cl}$ in the presence of $\mathrm{K_2CO_3}$ (see ESI† for full details and characterization).[23] Cluster synthesis was accomplished by reduction of complex **2a** with $\mathrm{NaBH_4}$ followed by etching with HCl. This procedure afforded cluster [**3a**]Cl_3 in 43% isolated yield based on Au, after purification by column chromatography (Fig. 2A).

The effect of HCl on the synthetic protocol was examined by UV-vis spectroscopy and electrospray ionization mass spectrometry (ESI-MS). The absorbance spectra of the cluster were significantly sharper after HCl etching, consistent with the size-focusing effect observed in other systems (Fig. S1†).[11,18] The molecular formula of the cluster [**3a**]Cl_3 was confirmed by ESI-MS, which showed a dominant molecular ion peak at 1741.26 *m*/*z* corresponding to $[\mathrm{Au}_{13}(\mathrm{bisNHC}^{\mathrm{Bn}})_5\mathrm{Cl}_2]^{3+}$ (Fig. 2B). Good agreement was observed between the experimental and theoretical isotopic distribution patterns. A minor peak at 2629.89 *m*/*z* was also observed, corresponding to the divalent ion $[\mathrm{Au}_{13}(\mathrm{bisNHC}^{\mathrm{Bn}})_5\mathrm{Cl}_2]\mathrm{Cl}^{2+}$ derived from incomplete ionization of the parent cluster.

The UV-vis spectrum of [**3a**]Cl_3 in dichloromethane shows distinct absorption bands at 324, 409, 456, and 511 nm (Fig. 2C, red), which are in line with previously reported Au_{13} clusters.[18] Solutions of [**3a**]Cl_3 in dichloromethane show bright red-orange emission. Photoluminescence quantum yields measured by two independent methods is 23%, a value considerably higher than most superatom gold clusters, including our previous report of 16% for an NHC-protected Au_{13} cluster.[18] The spectrum produced by excitation at 784 nm (Fig. 2C, black) is in good agreement with the UV-vis spectrum, supporting the conclusion that the measured quantum yield was not affected by contamination with other emissive species. Although the precise reason for the high quantum yield is currently under investigation, the rigid shell provided by the NHC with multiple π–π stacking interactions likely contributes.

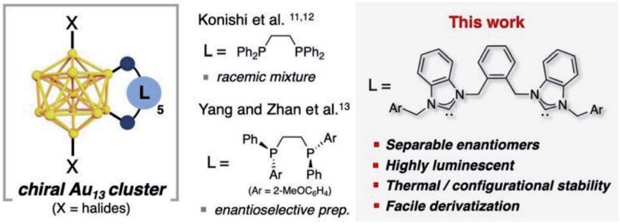

Fig. 1 Synthesis of chiral Au_{13} clusters.

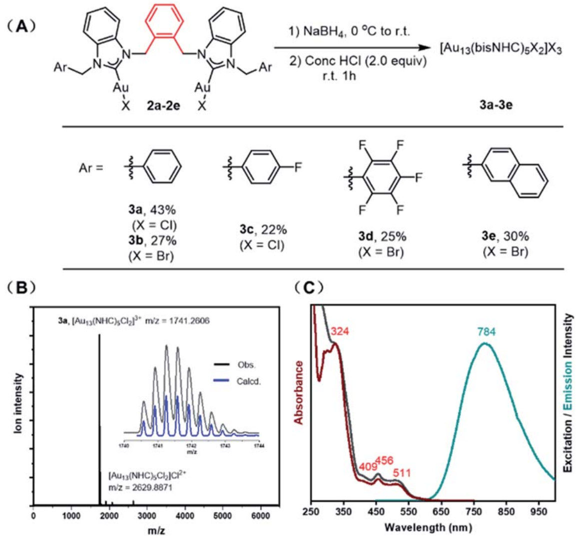

Fig. 2 (A) Preparation of $[\mathrm{Au}_{13}(\mathrm{bisNHC})_5\mathrm{X}_2]\mathrm{X}_3$ nanoclusters [**3a–e**]X_3 (B) ESI-MS of [**3a**]Cl_3; (C) UV-vis absorbance (red), photoluminescence excitation (black) and emission (green) spectra of [**3a**]Cl_3 in dichloromethane.

Halide counterions had little effect on cluster formation, with bromide complex **2b** affording 27% yield of $[\mathrm{Au}_{13}(\mathrm{bisNHC}^{\mathrm{Bn}})_5\mathrm{Br}_2]\mathrm{Br}_3$ ([**3b**]Br_3) after purification. The nature of the linking unit was found to be critically important, with *meta*- and *para*-xylyl linked ligands (**1f** and **1g** respectively) giving no observable Au_{13} clusters (see Fig. S2†). However, wingtip aromatic substituents were readily interchangeable, with complexes **2c–e** all affording Au_{13} nanoclusters (see ESI† for full characterization).

Single crystals of [**3a**]Cl_3 suitable for X-ray crystallography were grown from layering hexane onto a dichloromethane solution of the pure cluster. The structure features an icosahedral Au_{13} core with Au–Cl bonds capping the top and bottom of the core and the five bis-NHC ligands bound to the two twisted Au_5 pentagons of the core (Fig. 3). The average Au–C bond length is 2.05(2) Å, similar to other NHC-stabilized nanoclusters.[18] The average Au centre–Au peripheral bond distance of the icosahedral core is 2.7655(12) Å, and the average Au–Cl bond length of the terminal chloride ligands is 2.332(6) Å. A distinct structural characteristic is the face-to-face arrangement

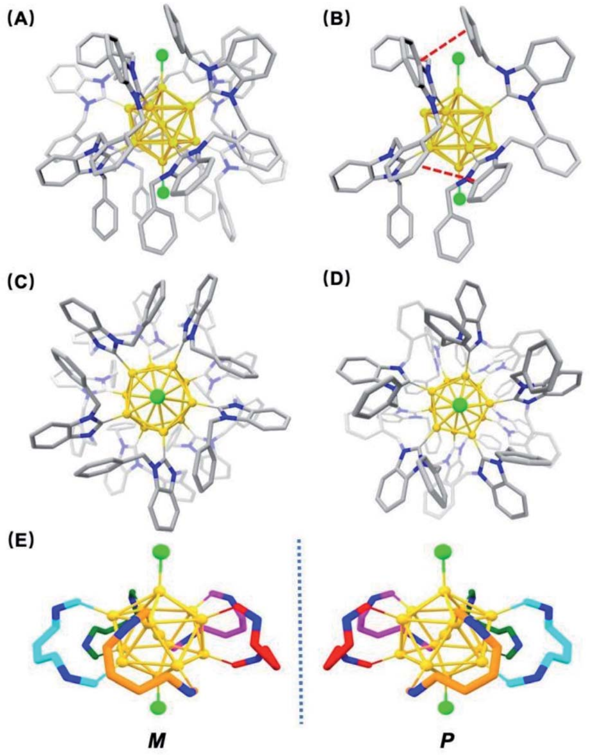

Fig. 3 (A) Single-crystal X-ray structure of [$Au_{13}(bisNHC^{Bn})_5Cl_2$]$Cl_3$ ([**3a**]Cl_3). Anions and hydrogen atoms have been removed for clarity (color key: carbon, gray; nitrogen, blue; chlorine, green; gold, yellow); (B) side-view of structure showing interactions between benzimidazole/*o*-phenyl bridge and benzimidazole/benzyl arm phenyl rings on neighbouring ligands; (C) top-down and (D) bottom-up views of the structure. See ESI† for full ORTEP structures; (E) *M*/*P* descriptors of **3a**. The chirality can be easily viewed from the left (counter-clockwise) and right (clockwise)-handed arrangement of the bisNHC ligand on the Au surface (dark blue: nitrogen of NHC).

of one benzimidazole and the *ortho*-phenyl bridge, and the other benzimidazole and one benzyl phenyl ring on neighbouring ligands, with average distances of 3.3 Å and 3.4 Å, respectively, suggesting the presence of π–π stacking interactions (Fig. 3B).

From the top view, the disposition of these mutually interacted components is unidirectional, rendering the top of **3a** different from the bottom. The NHC ligands are oriented with pseudo C_5 symmetry (Fig. 3C and D). From the bottom view, benzyl arms are oriented vertically without any possible interactions with the other components (Fig. 3D). Accordingly, **3a** has a helical chirality with pseudo C_5 symmetry (Fig. 3E). Cluster [**3a**]Cl_3 was crystallized as a racemic mixture in $Pna2_1$ space group with mirror planes.

To investigate whether this structure is conserved in solution, the clusters were characterized by NMR spectroscopy. The ^1H NMR spectrum of cluster [**3a**]Cl_3 has four sets of diastereotopic methylene CH_2 protons attributed to the benzyl and xylyl groups (Fig. 4A). This suggests a single ligand environment without C_2 symmetry and with a low degree of rotational freedom, similar to what is observed in the solid-state (see ESI† for full spectral details of all clusters). The NMR shifts of some protons were also found to be anion dependent, with [**3a**][PF_6]$_3$ displaying significant changes in methylene resonance shifts compared to the chloride analogue (see ESI† for full details).

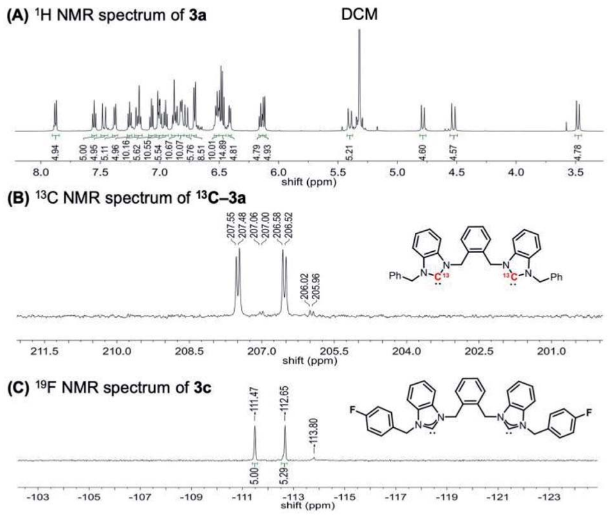

Fig. 4 Solution structural characterization of [$Au_{13}(bisNHC^{Ar})_5Cl_2$]$Cl_3$ clusters by NMR spectroscopy in CD_2Cl_2. (A) ^1H NMR spectrum of [**3a**]Cl_3. (B) Cluster region of the $^{13}C\{^1H\}$ NMR spectrum of ^{13}C-[**3a**][PF_6]$_3$ bearing ^{13}C(C2)-labelled bisNHC ligand; (C) ^{19}F NMR spectrum of [**3c**]Cl_3 (the signal at 113.80 ppm belongs to a small amount of [L_2Au_2]Cl_2).

The asymmetric ligand environment was also confirmed by synthesizing ^{13}C-labeled cluster ^{13}C-[**3a**][PF_6]$_3$ using $^{13}C(C_2)$-labelled NHC precursor, which enables the direct observation of the M–C bond. The $^{13}C\{^1H\}$ NMR spectrum has two major carbene peaks, which appear as doublets at 207.5 and 206.6 ppm (Fig. 4B). A minor set of two doublets was also observed at 207.0 and 206.0 ppm, the origin of which is currently under further study in our group. Similarly, the ^{19}F NMR spectrum of the fluorinated analogue [**3c**]Cl_3 displays two signals at −111.5 and −112.7 ppm (Fig. 4C).

Thus, solution NMR spectroscopic results support the presence of ligand asymmetry in solution as well as solid state. The NMR studies are also consistent with conformational rigidity of the clusters, at least on the NMR timescale, as we have reported previously for other related NHC-functionalized clusters.[18] These results suggested that the clusters might have high configurational stability, such that the separation of the two enantiomers *via* solution-based methods, such as chiral HPLC, might be feasible.

With solution NMR studies showing high structural rigidity of the cluster, we then proceeded to attempt to separate the two enantiomers. [**3a**]Cl_3 was successfully separated into its constituent enantiomers using a chiral cellulose-based analytical HPLC column with methanol (MeOH) as the eluent, along with trifluoroacetic acid (TFA) and diethylamine (DEA) as additives. Two well-separated peaks were observed at 21.6 and 24.2 minutes in an approximately 1 : 1 ratio as expected for a racemic mixture (labelled as enantiomers **3a**-en1 and **3a**-en2 respectively, Fig. 5A). These conditions enabled the separation of a large batch (20 mg) of racemic cluster [**3a**]Cl_3 by preparative

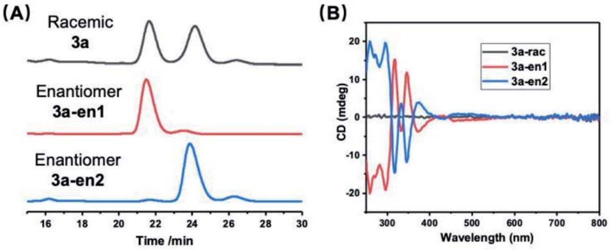

Fig. 5 Enantioseparation and characterization of chiral Au_{13} nanoclusters: (A) chromatogram showing the enantioseparation of *rac*-**3a** by chiral HPLC using UV-vis detection at 350 nm; (B) CD spectra of the two chiral enantiomers separated by HPLC and *rac*-**3a** for comparison.

chiral HPLC. The enantiomeric excess (ee) of the two collected fractions was determined by chiral HPLC and found to be 88% for **3a**–en1 and 95% for **3a**-en2. The UV-vis, NMR and mass spectra of the separated enantiomers were consistent with the starting racemic mixture, illustrating the stability of the Au_{13} structure under the separation conditions, although the ESI-MS and NMR spectra suggest that anion exchange with trifluoroacetate anion had occurred (Fig. S3–S5†).

The as-separated enantiomers were characterized by circular dichroism (CD) spectroscopy (Fig. 5B). As expected, the CD spectra of the two enantiomers are mirror images and show distinct bands between 250 and 800 nm (main peaks: 259, 271, 296, 317, 333 nm, weak peaks at 376, 425 nm, and a broad peak at 500 nm). No CD signal was observed for the racemic mixture.

The thermal stability of cluster [**3a**]Cl_3 was investigated by UV-vis spectroscopy. The UV-vis spectrum showed no discernible change after 3 days of heating at 60 °C in acetonitrile (Fig. 6A). Emission spectra were also identical within error after this time (Fig. S7†). The configurational stability of **3a** was investigated by monitoring the change in enantiopurity upon heating to different temperatures. Samples of **3a**-en1 (88% initial ee) were heated in MeOH at a variety of temperatures for 1 h. At 60 °C, there was no discernible change, but a slight drop to 81% ee was observed when the cluster was heated to 80 °C, and at 100 °C the ee further decreased to 72% (Fig. 6B). Changes in enantiomeric ratios were documented by HPLC (Fig. S8†) and CD (Fig. S9†). Work to clarify the mechanism of racemization is underway in our lab.

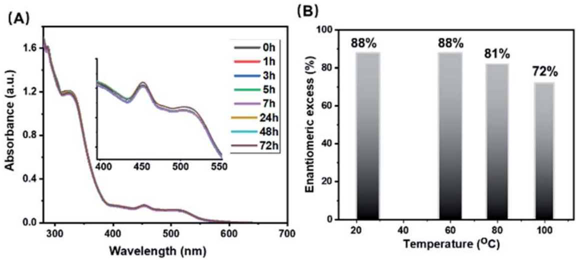

Fig. 6 (A) Thermal stability of *rac*-**3a** at 60 °C in acetonitrile monitored by UV-vis spectroscopy; (B) chiral stability of **3a-en-1** in methanol after treatment at different temperatures for 1 h. The enantiomeric purity after heating was examined by chiral HPLC.

Conclusions

In conclusion, we have described the synthesis and structural characterization of a new chiral *ortho*-xylyl linked bisNHC-stabilized Au_{13} cluster $[Au_{13}(bisNHC^{Bn})_5Cl_2]Cl_3$ ([**3a**]Cl_3) and its bromide derivative [**3b**]Br_3. These clusters have a similar icosahedral structure to previously reported Au_{13} clusters, including those ligated by monodentate,[18] bis-NHC[19] and bisphosphine ligands.[11] A variety of wingtip groups were compatible with nanocluster formation, allowing for the isolation of clusters incorporating diverse functionality (**3c–e**). The chirality of cluster **3a** in the solid-state was investigated by X-ray crystallography, where it was discerned that chirality results from a helical arrangement of the surface ligands that is dictated by the choice of a bidentate ligand. The two enantiomers were separated by chiral HPLC and characterized by CD spectra. The clusters show high thermal stability and stability against racemization, which may facilitate their future applications in chiral catalysis and sensing.

Data availability

The experimental data is included in the ESI.

Author contributions

C. C. and M. N. conceived the project. H. Y. and K. O. carried out the synthesis, purification and characterization of the Au_{13} nanoclusters. T. L. performed the quantum yield of Au_{13} nanocluster. A. V., Y. A., and T. O. analysed the X-ray crystal of the cluster [**3a**]Cl_3. All the authors wrote the paper, supplementary methods, and related materials.

Conflicts of interest

The authors declare no competing financial interests.

Acknowledgements

This work was supported by KAKENHI from JSPS (17H03030 to C. M. C.). H. Y. and K. M. O. thank JSPS for funding through the JSPS International Research Fellow program. M. N. thanks the support from The Mazda foundation. A. J. V. thanks NSERC for a Vanier Scholarship and the Walter C. Sumner foundation for additional scholarship support. T. I. L. thanks NSERC for a postdoctoral fellowship. We thank DAICEL corporation for the assistance of separation of enantiomers. JSPS and NU are acknowledged for funding of this research through The World Premier International Research Centre Initiative (WPI) program. NSERC and the Canada Foundation for Innovation (CFI) are thanked for financial support of this work in terms of operating and equipment grants to C. M. C. The authors thank Dr Kevin Stamplecoskie (Queen's University) for access to UV-vis absorbance and fluorescence spectrometers and for useful advice on fluorescence quantum yield measurements.

References

1 (*a*) S. Knoppe and T. Burgi, *Acc. Chem. Res.*, 2014, **47**, 1318–1326; (*b*) Y. Zhu, J. Guo, X. Qiu, S. Zhao and Z. Tang, *Acc. Mater. Res.*, 2020, **2**, 21–35; (*c*) Y. Li, T. Higaki, X. Du and R. Jin, *Adv. Mater.*, 2020, **32**, e1905488; (*d*) C. Zeng and R. Jin, *Chem.–Asian J.*, 2017, **12**, 1839–1850; (*e*) Q.-Y. Zhang and L. Zhao, *Tetrahedron Lett.*, 2018, **59**, 310–316.

2 D. Astruc, M. C. Daniel and J. Ruiz, *Chem. Commun.*, 2004, 2637–2649.

3 (*a*) T. Mallat, E. Orglmeister and A. Baiker, *Chem. Rev.*, 2007, **107**, 4863–4890; (*b*) E. S. Andreiadis, M. R. Vitale, N. Mezailles, X. Le Goff, P. Le Floch, P. Y. Toullec and V. Michelet, *Dalton Trans.*, 2010, **39**, 10608–10616.

4 (*a*) Y. Zhao, M. A. Belkin and A. Alu, *Nat. Commun.*, 2012, **3**, 870; (*b*) L. Ohnoutek, N. H. Cho, A. W. Allen Murphy, H. Kim, D. M. Rasadean, G. D. Pantos, K. T. Nam and V. K. Valev, *Nano Lett.*, 2020, **20**, 5792–5798.

5 (*a*) A. Lechtken, D. Schooss, J. R. Stairs, M. N. Blom, F. Furche, N. Morgner, O. Kostko, B. von Issendorff and M. M. Kappes, *Angew. Chem., Int. Ed.*, 2007, **46**, 2944–2948; (*b*) X. K. Wan, S. F. Yuan, Z. W. Lin and Q. M. Wang, *Angew. Chem., Int. Ed.*, 2014, **53**, 2923–2926.

6 (*a*) T. G. Schaaff and R. L. Whetten, *J. Phys. Chem.*, 2000, **104**, 2630–2641; (*b*) H. Yao, K. Miki, N. Nishida, A. Sasaki and K. Kimura, *J. Am. Chem. Soc.*, 2005, **127**, 15536–15543; (*c*) Y. Yanagimoto, Y. Negishi, H. Fujihara and T. Tsukuda, *J. Phys. Chem. B*, 2006, **110**, 11611–11614.

7 (*a*) O. Lopez-Acevedo, H. Tsunoyama, T. Tsukuda, H. Hakkinen and C. M. Aikens, *J. Am. Chem. Soc.*, 2010, **132**, 8210–8218; (*b*) C. Zeng, T. Li, A. Das, N. L. Rosi and R. Jin, *J. Am. Chem. Soc.*, 2013, **135**, 10011–10013.

8 (*a*) I. Dolamic, S. Knoppe, A. Dass and T. Burgi, *Nat. Commun.*, 2012, **3**, 798; (*b*) S. Knoppe, I. Dolamic, A. Dass and T. Burgi, *Angew. Chem., Int. Ed.*, 2012, **51**, 7589–7591.

9 S. Knoppe, I. Dolamic and T. Burgi, *J. Am. Chem. Soc.*, 2012, **134**, 13114–13120.

10 S. Malola and H. Häkkinen, *J. Am. Chem. Soc.*, 2019, **141**, 6006–6012.

11 Y. Shichibu and K. Konishi, *Small*, 2010, **6**, 1216–1220.

12 (*a*) J. Zhang, Y. Zhou, K. Zheng, H. Abroshan, D. R. Kauffman, J. Sun and G. Li, *Nano Res.*, 2018, **11**, 5787–5798; (*b*) Y. Shichibu, Y. Ogawa, M. Sugiuchi and K. Konishi, *Nanoscale Adv.*, 2021, **3**, 1005–1011.

13 Y. Yang, Q. Zhang, Z. J. Guan, Z. A. Nan, J. Q. Wang, T. Jia and W. W. Zhan, *Inorg. Chem.*, 2019, **58**, 3670–3675.

14 (*a*) C. M. Crudden, J. H. Horton, I. I. Ebralidze, O. V. Zenkina, A. B. McLean, B. Drevniok, Z. She, H. B. Kraatz, N. J. Mosey, T. Seki, E. C. Keske, J. D. Leake, A. Rousina-Webb and G. Wu, *Nat. Chem.*, 2014, **6**, 409–414; (*b*) A. V. Zhukhovitskiy, M. J. MacLeod and J. A. Johnson, *Chem. Rev.*, 2015, **115**, 11503–11532; (*c*) S. Engel, E. C. Fritz and B. J. Ravoo, *Chem. Soc. Rev.*, 2017, **46**, 2057–2075; (*d*) G. Wang, A. Ruhling, S. Amirjalayer, M. Knor, J. B. Ernst, C. Richter, H. J. Gao, A. Timmer, H. Y. Gao, N. L. Doltsinis, F. Glorius and H. Fuchs, *Nat. Chem.*, 2017, **9**, 152–156; (*e*) C. A. Smith, M. R. Narouz, P. A. Lummis, I. Singh, A. Nazemi, C. H. Li and C. M. Crudden, *Chem. Rev.*, 2019, **119**, 4986–5056.

15 (*a*) C. M. Crudden and D. P. Allen, *Coord. Chem. Rev.*, 2004, **248**, 2247–2273; (*b*) T. J. Robilotto, J. Bacsa, T. G. Gray and J. P. Sadighi, *Angew. Chem., Int. Ed.*, 2012, **51**, 12077–12080; (*c*) M. N. Hopkinson, C. Richter, M. Schedler and F. Glorius, *Nature*, 2014, **510**, 485–496; (*d*) L. Jin, D. S. Weinberger, M. Melaimi, C. E. Moore, A. L. Rheingold and G. Bertrand, *Angew. Chem., Int. Ed.*, 2014, **53**, 9059–9063.

16 (*a*) T. H. Tsukuda and H. Häkkinen, *Protected Metal Clusters: From Fundamentals to Applications*, Elsevier, Amsterdam, 2015; (*b*) Q. Tang, G. Hu, V. Fung and D. E. Jiang, *Acc. Chem. Res.*, 2018, **51**, 2793–2802; (*c*) J. Yan, B. K. Teo and N. Zheng, *Acc. Chem. Res.*, 2018, **51**, 3084–3093; (*d*) I. Chakraborty and T. Pradeep, *Chem. Rev.*, 2017, **117**, 8208–8271; (*e*) R. Jin, C. Zeng, M. Zhou and Y. Chen, *Chem. Rev.*, 2016, **116**, 10346–10413; (*f*) X. Kang, Y. Li, M. Zhu and R. Jin, *Chem. Soc. Rev.*, 2020, **49**, 6443–6514; (*g*) Z. Lei, X. L. Pei, H. Ube and M. Shionoya, *Bull. Chem. Soc. Jpn.*, 2021, **94**, 1324–1330.

17 M. R. Narouz, K. M. Osten, P. J. Unsworth, R. W. Y. Man, K. Salorinne, S. Takano, R. Tomihara, S. Kaappa, S. Malola, C. T. Dinh, J. D. Padmos, K. Ayoo, P. J. Garrett, M. Nambo, J. H. Horton, E. H. Sargent, H. Hakkinen, T. Tsukuda and C. M. Crudden, *Nat. Chem.*, 2019, **11**, 419–425.

18 M. R. Narouz, S. Takano, P. A. Lummis, T. I. Levchenko, A. Nazemi, S. Kaappa, S. Malola, G. Yousefalizadeh, L. A. Calhoun, K. G. Stamplecoskie, H. Hakkinen, T. Tsukuda and C. M. Crudden, *J. Am. Chem. Soc.*, 2019, **141**, 14997–15002.

19 H. Shen, S. Xiang, Z. Xu, C. Liu, X. Li, C. Sun, S. Lin, B. K. Teo and N. Zheng, *Nano Res.*, 2020, **13**, 1908–1911.

20 (*a*) H. Shen, G. Deng, S. Kaappa, T. Tan, Y. Z. Han, S. Malola, S. C. Lin, B. K. Teo, H. Hakkinen and N. Zheng, *Angew. Chem., Int. Ed.*, 2019, **58**, 17731–17735; (*b*) H. Shen, Z. Xu, M. S. A. Hazer, Q. Wu, J. Peng, R. Qin, S. Malola, B. K. Teo, H. Hakkinen and N. Zheng, *Angew. Chem., Int. Ed.*, 2021, **60**, 3752–3758.

21 K. Hirano, S. Takano and T. Tsukuda, *J. Phys. Chem. C*, 2021, **125**, 9930–9936.

22 P. Luo, S. Bai, X. Wang, J. Zhao, Z. N. Yan, Y. F. Han, S. Q. Zang and T. C. W. Mak, *Adv. Opt. Mater.*, 2021, 2001936.

23 A. Collado, A. Gomez-Suarez, A. R. Martin, A. M. Slawin and S. P. Nolan, *Chem. Commun.*, 2013, **49**, 5541–5543.